The Experiment for Space Radiation Analysis (ESRA): Technology Maturation of Next Generation Charged Particle Detectors in GTO

Carlos Maldonado, August Gula, Martin Kroupa, Jonathan Barney, Michael Caffrey, Susan Mendel, Rachel Simms, Kerry Boyd, Zachary Miller, Justin McGlown, Jonathan Deming, Kim Katko, Markus Hehlen, Brooke Mosley, Justin Tripp, Keith Morgan, John Michel, Anthony Nelson, Robert Merl, Michael Holloway, Heidi Morning, Daniel Arnold, Ruth Skoug, Phil Fernandes, Ted Schultz, Angus Guider, Daniel Reisenfeld, Brian Larsen, John Steinberg, Erik Krause, Darrel Beckman, Benigno Sandoval, Paul Graham, Zephram Tripp, Bradley Hoose, Rory Scobie, Joshua Ortner, Quinten Cole, Thomas Fairbanks, Jeffrey George, Rustam Niyazov, Robert Clanton, Andrew Kirby, J.P. Martinez, Tracy Gambill, Melissa Ma, Kasidit Subsomboon, Darren Harvey, Katherine Alano, Kristina McKeown, and Donathan Ortega

Los Alamos National Laboratory

ABSTRACT

The Experiment for Space Radiation Analysis (ESRA) is the latest Demonstration and Validation mission built by the Los Alamos National Laboratory, with a focus on testing next generation plasma and energetic particle sensors. The primary motivation for the ESRA payloads is to minimize size, weight, power, and cost while still providing necessary mission data. These new instruments will be demonstrated by ESRA through testing and on-orbit operations to increase their technology readiness level such that they can support the evolution of technology and mission objectives. This project will leverage a commercial off-the-shelf CubeSat bus along with commercial satellite ground networks to reduce the cost and timeline associated with traditional DemVal missions. The system will launch as a ride share with the DoD Space Test Program to be inserted in Geosynchronous Transfer Orbit and allow observations of the Earth's radiation belts. The ESRA mission consists of two science payloads and several subsystems: the Wide-field-of-view Plasma Spectrometer, the Energetic Charged Particle telescope, high voltage power supply, payload processor, flight software architecture, and distributed processor module. The ESRA CubeSat will provide measurements of the plasma and energetic charged particle populations in the GTO environment for ions ranging from ~100 eV to ~1000 MeV and electrons with energy ranging from 100 keV to 20 MeV.

1. INTRODUCTION

Historically, space plasma and energetic charged particle instrument design has been guided by the philosophy of "build to performance" however while these heritage instruments have been exquisite, in both design and capability, the measurement sensitivity comes at a steep cost [1]. Over the years this design paradigm has resulted in increased instrument cost and resource requirements to the point that they are not attractive options for smaller missions operating under ever increasing fiscal constraints. This is particularly the case for implementation as science payloads of mega constellations required for ubiquitous multi-point space plasma measurements [2, 3]. The current space physics era of dwindling budgets coupled with ever expanding CubeSat launch opportunities has revitalized the demand for low-resource instruments that can yield relevant science return [4, 5, 6]. As the space physics community seeks to leverage increasingly sophisticated CubeSat platforms, with their frequent rideshare options and ability to provide spatial and temporal measurements at a much-reduced cost, there has been an increased focus in the development of miniaturized instruments [7, 8, 9, 10]. This interest, combined with advances in sensor and other spacecraft technologies, has enabled the rapid increase in the number of miniaturized charged particle detectors with flight heritage. Examples include retarding potential analyzers [11], laminated electrostatic analyzers [12, 13, 14, 15, 16], ion mass spectrometers [17, 18, 8], traditional spherical analyzers [19], and charged particle telescopes [20, 21, 22, 23]. The parallel advancements in both CubeSat platforms and miniaturized sensors allows for high quality observations of the dynamic space environment, to provide charged particle distribution measurements from which can be obtained the kinetic energy, temperature, and density, along with the resulting spacecraft–environment interaction effects of a multitude of environments. The benefits of such measurements include an increased

understanding of the physical phenomena and processes concerning solar wind, magnetospheric and ionospheric science, local space weather forecasting, and spacecraft anomaly resolution.

Recent years have witnessed a tremendous growth in satellite constellations for scientific [24, 25, 26], commercial [27, 28], and government applications [29]. Readily identifiable challenges with implementing a large or even mega-constellation of small satellites or CubeSats for scientific missions are: (1) the satellite bus must be sophisticated such that it can support the appropriate sensors and subsystems while operating in the required space environments and (2) the sensors must fit within constrained resource limits, i.e. reduced in size, weight, power, and cost (SWAP-C), while still providing the ability to make the required measurements. The first challenge includes the platform's ability to support mission requirements such as power generation, pointing accuracy, slew rate, along with the ability to survive and operate in the natural space radiation environment. The survivability requirement poses a significant technical challenge since the mass and volume constraints of CubeSats present considerable challenges in terms of supporting radiation shielding. However, engineering solutions such as appropriate electronics part selection, spot shielding, and software techniques to mitigate single-event-upsets (SEUs) offer attractive engineering solutions for CubeSat missions targeting environments beyond low-Earth orbit (LEO) [30, 22, 31].

2. ESRA MISSION OVERVIEW

The Experiment for Space Radiation Analysis (ESRA) is the latest Demonstration and Validation (DemVal) mission built by the Los Alamos National Laboratory (LANL), to design, develop, and fly next generation plasma and energetic particle sensors [31, 32]. The primary motivation for the ESRA payloads is to minimize SWAP-C while still providing necessary observations of the local space environment. These new instruments will be demonstrated by ESRA through testing and on-orbit operations to rapidly increase their technology readiness level (TRL) such that they can support the evolution of technology and mission objectives. This project will leverage a commercial off-the-shelf (COTS) CubeSat bus along with commercial satellite ground networks to reduce the cost and timeline associated with traditional DemVal missions. By partnering with, and leveraging commercial sector expertise, LANL staff can focus solely on payload development thus minimizing cost and risk. The system will launch as a ride share with the DoD Space Test Program (STP) to be inserted in Geosynchronous Transfer Orbit (GTO) and allow observations of the Earth's radiation belts.

The ESRA mission consists of two science payloads and several novel subsystems: the Wide-field-of-view Plasma Spectrometer (WPS), the Energetic Charged Particle (ECP) telescope, high voltage power supply (HVPS), payload processor, flight software architecture, and distributed processor module (DPM). The ESRA CubeSat will provide measurements of the plasma and energetic charged particle populations in the GTO environment for ions ranging from ~100 eV to 30 keV and 100 keV to ~1000 MeV and electrons with energy ranging from 100 keV to 20 MeV. ESRA will additionally demonstrate the potential of CubeSats for both science and space weather monitoring in the radiation belts, serving as a pathfinder to future constellation type missions beyond LEO. To date, there have been no successful CubeSat missions through the radiation belts reported in the open literature. A 6U CubeSat mission to geostationary transfer orbit, called GTOSat [22], is scheduled for launch in 2022. This mission will measure energetic electrons and protons at a reduced energy range (when compared to ESRA) from ~hundreds of keV to a few MeV. By using a commercial 12U bus, ESRA will, for the first time, demonstrate a low-cost, rapidly deployable spaceflight platform with sufficient SWAP to enable efficient measurements of the energetic particle populations in the dynamic radiation belts.

A 12U commercial satellite bus provided by NanoAvionics will serve as the platform for the WPS and ECP sensors along with the critical subsystems such as the HVPS, DPM, and Payload Processor. The avionics and critical subsystems have flight heritage from the M6P mission. With already more than 75 successful satellite missions and satellite-related commercial projects, NanoAvionics will assemble the 12U bus at its facilities, while the final integration of the payload will be carried out at LANL facilities. The 12U bus matches LANL's mission requirements and shares the same flight-proven subsystems as NanoAvionics' flagship M6P bus, but with up to 10U payload volume. The larger volume will be necessary to provide enough room for the ~10 kg payload that includes the WPS and ECP sensors as well as the critical subsystems. The mission launch and integration are being provided by the DoD Space Test Program with an anticipated GTO insertion. The desired orbital parameters include perigee of 200 km, apogee of 36,000 km, and inclination of 40° ±20°, with an anticipated ready for launch date of September 1, 2024. The final apogee and perigee will be selected such that the ESRA vehicle will naturally de-orbit within the 25-year lifetime requirement. The solar cycle is heading towards a period of maximum activity in 2024 and the initial orbital

modeling indicates that ESRA will readily meet the de-orbit requirement. Once the initial on-orbit checkout and commissioning activities have been completed the science operations will commence. The configuration of the sensors and platform has been designed so that while the double deployable solar panels are facing the Sun and actively charging, the WPS sensor will not be facing directly at the Sun and the ECP sensor will be facing roughly perpendicular to the magnetic field lines. Note, in general plasma spectrometers such as WPS are not pointed directly at the Sun due to UV photon contamination of the detector [33, 34, 35, 36]. The ESRA CAD model is shown in Fig. 1, with payloads and subsystems indicated.

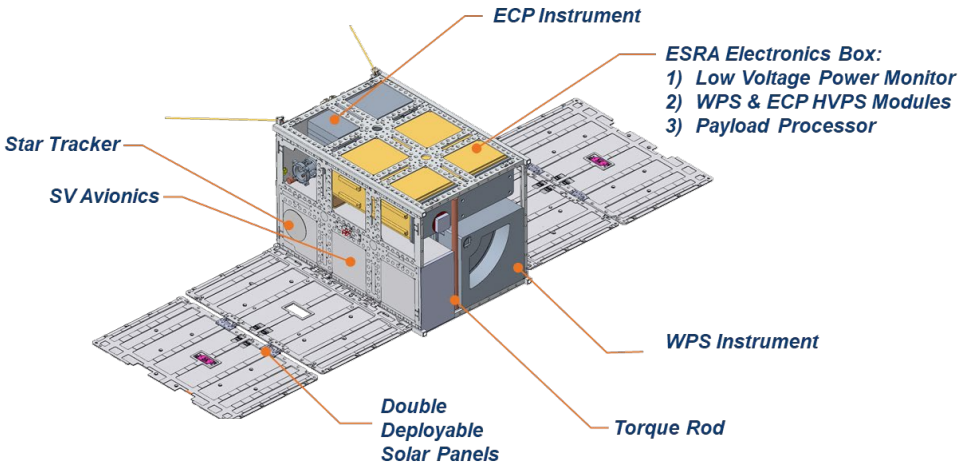

Fig. 1. CAD model of the ESRA flight vehicle.

3. ENERGETIC CHARGED PARTICLE TELESCOPE

The Energetic Charged Particle (ECP) telescope measures protons and electrons over a broad range of energies (100 keV – 1000 MeV for protons, and 100 keV – 20 MeV for electrons). The telescope design incorporates a stack of five detectors: two thin Si detectors (80 μm), two thick Si detectors (1.5 mm), and one GAGG(Ce) (Ce^{3+}-doped $Gd_3Al_2Ga_3O_{12}$) scintillator (1 cm) with a Hamamatsu S3590-08 PhotoDiode (PD). The computer aided design (CAD) model of the ECP telescope is shown in Fig. 2. To minimize background counts due to penetrating radiation, the sensitive detectors in the telescope are shielded with tungsten (grey) and aluminum (yellow). To further decrease the background signal and improve signal to noise ratio of the telescope, an aluminum collimator with tungsten discs is positioned in front of the telescope. Higher stopping-power CZT detectors in the concept design were replaced with silicon to save protracted development of the CZT readout to handle charge collection issues [37, 38].

Each detector channel has dedicated read-out electronics which are integrated within the instrument housing. Three electronic boards comprise each electronics module and are optimized to fit the allocated footprint while minimizing noise and heat cross-talk. The board closest to the detectors is the Sensor Interface Board (SIB) which provides a low-noise interface between the electronics and detectors. The SIB also provides detector biasing and monitors the leakage current. The Front-End Electronics (FEE) board incorporates junction-gate field-effect transistors and charge sensitive preamplifiers to amplify detector signals. After the amplified signals are shaped and filtered, each signal is then sampled by an analog-to-digital converter (ADC) with a sampling rate of 80 MHz. This digital signal is passed to the Distributed Processing Module (DPM) where a field-programmable gate array (FPGA) analyzes the signal. Compared to the standard application with the "peak hold" approach, this fully digital approach enables much more sophisticated signal processing, resulting in higher acceptable count rate due to "in-flight" baseline restoration.

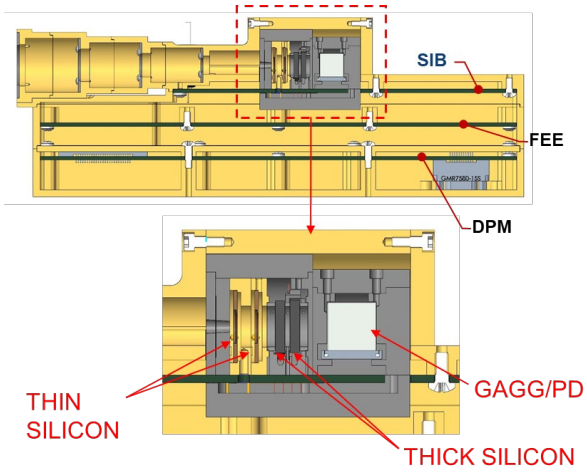

Fig. 2. CAD model cutaway of the ESRA ECP telescope.

The ECP is designed to make both energy and Particle ID (PID) determination using combined information from deposited energies in the detector. In an effort to evaluate the detection efficiency, a Geant4 [39] simulation is performed with protons and electrons flux directed into the entrance aperture over a range of angles. The results are analyzed using a logical reconstruction analysis, with proton bins considered first, and if no match is found, electron bins are then considered. The detection efficiency can be neatly summarized using "bowtie" plots, as shown in Fig. 3 for protons. Each energy bin is represented with a different color, and the response for each energy bin is shown as a function of incident particle energy. The simulation and analysis of the ECP telescope is described in more detail by Barney et al. [38].

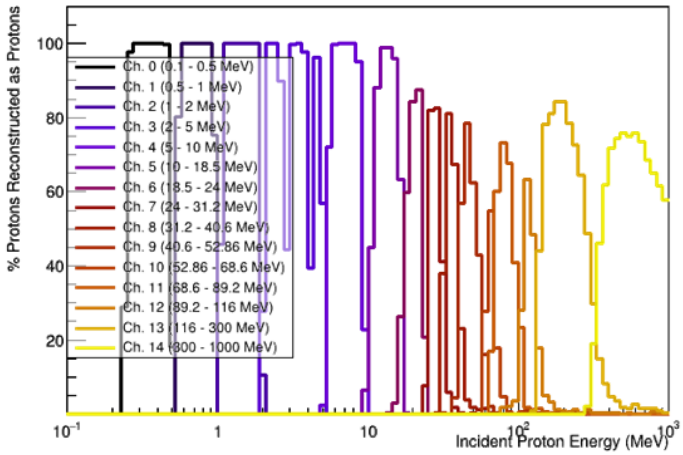

Fig. 3. Proton channel reconstruction efficiencies [38].

Prototyping of the full read-out electronics chain using radioisotope sources along with Si and GAGG detectors is being conducted to verify design performance. The thick silicon was mounted on the SIB board with a bias voltage of +200 V applied from an external ORTEC 556 high voltage power supply. The silicon detector and the SIB board were enclosed in an Electro-Magnetic Interference (EMI) shielded glovebox. The readout of this detector was pre-amplified with a CAEN A1422 and then amplified with an ORTEC 579 fast filter amplifier. This amplified pulse was then analyzed by an Amptek MCA-8000D "PocketMCA." The resulting spectrum shown in Fig. 4 was taken over an integration time of 2 hrs for a 133Ba calibration source. The calibration source was placed ~1 cm from the detector.

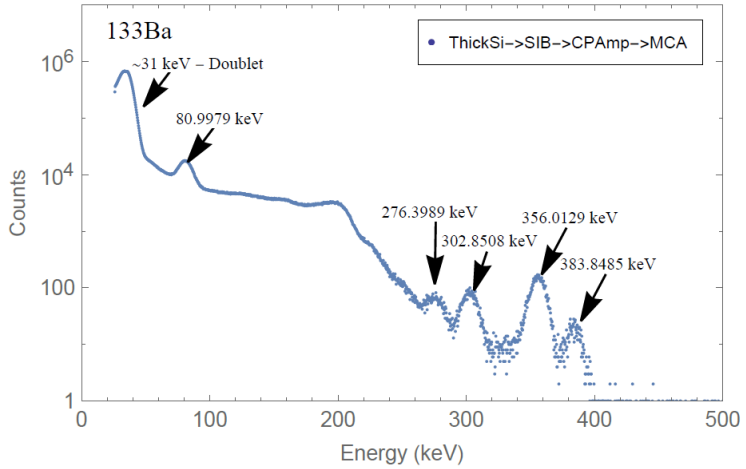

Fig. 4. Thick silicon detector calibration with 133Ba. The thick silicon was tested on the SIB board and readout through commercial (CPAmp->MCA) electronics.

The orange data shown in Fig. 5 for the GAGG detector used the same commercial electronics described above for the thick silicon detector. However, the GAGG was biased to +80 V. The orange data was taken over an integration time of 0.5 hrs using a 208Tl calibration source. The source was placed ~5 cm from the detector. The blue data shown in Fig. 5 was acquired using the GAGG and prototype sensor electronics enclosed in an EMI shielded glove box over a period of 90 hrs. The calibration source was placed at approximately the same distance as the previous run. The GAGG was powered by the same ORTEC 556 and the readout pulses were analyzed by the same PocketMCA mentioned previously.

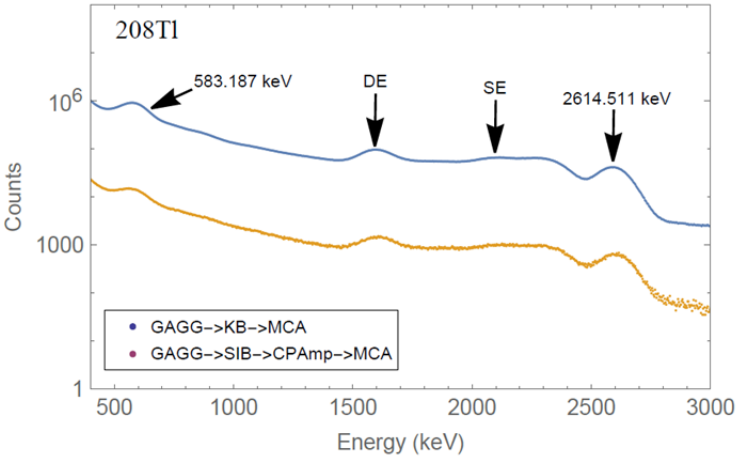

Fig. 5. GAGG Calibration with 208Tl. Two sets of data are shown for comparison and validation during the testing of ESRA-ECP electronics. Commercial electronics (CPAmp->MCA) and prototype electronics (KB) spectra are shown.

When fully built, we will calibrate the instrument utilizing both test pulses, radioactive sources, and high energy proton and electron beam lines. Pre-flight certification will be done in a proton beam where the performance of the instrument will be verified.

4. WIDE-FIELD-OF-VIEW PLASMA SPECTROMETER

The WPS is a novel plasma spectrometer based on a pinhole camera design concept that measures ion and electron energies over a broad field-of-view (FOV) without relying on spacecraft spin or deflection plates, both of which require time and/or additional resources to obtain full distribution measurements. The unique design enables a dramatic reduction of resources (SWAP-C) compared to cylindrical and spherical section analyzers and top hat designs. The WPS sensor is a revolutionary step forward in electrostatic analyzer design and is the ideal option for 3-axis stabilized spacecraft. The WPS instrument concept was first introduced in detail by Skoug, et al. [40] and we

briefly paraphrase their description here. Two subsystems comprise the WPS instrument: the sensor-head and the detector subsystems. The sensor head subsystem consists of the entrance aperture dome, the energy-angle (EA) charged particle filter plate, and the ogive structure at the center of the EA filter plate (see Fig. 6). The detector subsystem includes a transparent grid, microchannel plate (MCP) detector which detects individual particles, a position sensitive crossed delay line (XDL) anode, and associated front-end electronics (FEE).

The operation of WPS is shown schematically in Fig. 6 (left) following an ion as it travels from the entrance aperture to the 2D imaging anode. An ion enters the pinhole in the upper dome, held at spacecraft potential, with incident energy E_0, polar angle α_0, and azimuthal angle ϕ_0. The ion travels toward the EA filter plate and ogive structure that are held at a voltage bias V_{fp}. The ion is affected by the electric field created by the difference in potential between the upper dome and filter plate. The ion reaches the EA filter plate at radial distance r and angle β. The EA filter plate includes a series of slots whose bias angle b varies as a function of radius r. The ion then traverses the slot in the filter plate so long as $\beta = b$. Upon exiting the filter plate, the ion passes through the grid and the impact location is recorded using the MCP/XDL 2D imaging anode. The radial location maps to the incident polar angle of the ion α_0; the azimuthal location maps to the incident azimuthal angle of the ion ϕ_0; and the EA filter plate voltage V_{fp} maps to the incident energy of the ion E_0. The EA filter plate voltage V_{fp} is then swept over a range of voltages to obtain the full energy distribution of incident ions. In this way, (V_{fp}, r, β) from WPS maps to (E_0, α_0, ϕ_0) of the incident ion.

The modeled instrument response is obtained by means of the SIMION software package [41]. The cylindrical symmetry of the instrument allowed simulations to be performed in 2.5-D mode, in which a model is constructed in two dimensions and then rotated about the symmetry axis within SIMION to allow examination of the 3-D instrument response [42, 32]. The coordinate axes and definition of azimuth (ϕ) and elevation (θ) angles are shown schematically in Fig. 6 (right).

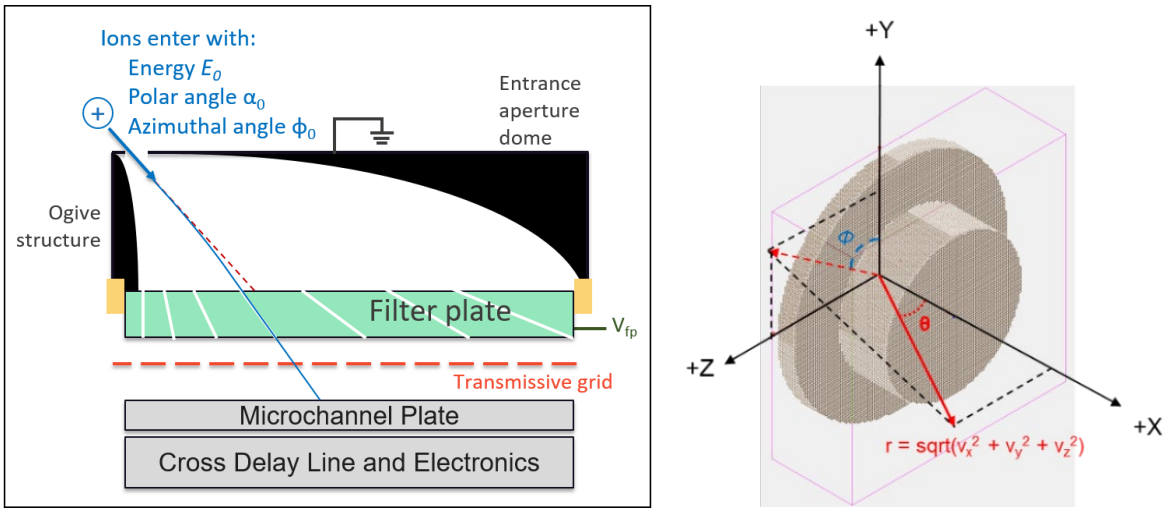

Fig. 6. Cartoon schematic of the WPS key elements and operation (left) and SIMION model of the full size WPS (right).

The location of the ions incident on the detector plane will be observed using an MCP stack followed by an XDL anode. The XDL sensors have an established history of use in space-based instruments for photon detection [43] [44] [45] [46] [47]. The XDL assembly consists of a standard MCP detector in a z-stack (3 plate) configuration followed by a cross delay-line anode. An incident ion strikes the front of the MCP detector and generates a secondary electron avalanche, resulting in a gain of ~10^7, which exits the MCP depositing the resulting charge on the anode. The XDL anode is formed by two orthogonal serpentine conductors and the position of the charge pulse is then determined by the difference in arrival time of the pulse at the ends of resistive-capacitance delay lines, shown schematically in Fig. 7. The XDL electronics consist of a high gain-bandwidth product operational amplifiers and fast comparators configured in a constant fraction discriminator (CFD) topology at the end of each delay line. This circuit amplifies the pulses from the XDL and translates the analog pulse to a digital signal to drive the start and stop inputs on the time-to-digital converter (TDC) integrated circuits. The advantage of utilizing CFD topology is to negate the effects of conventional threshold triggering which inherently introduces errors in timing measurements between analog input pulses of varying amplitudes. The CFD circuit behaves as an amplitude-invariant mechanism to drive the TDCs. The

resolution of the assembly will be determined by the event timing error which is dominated by the CFD performance46. An initial XDL sensor with dimensions of 94 mm × 94 mm has been selected for the WPS prototype with the majority of the electronics work being dedicated to the design and optimization of the supporting electronics.

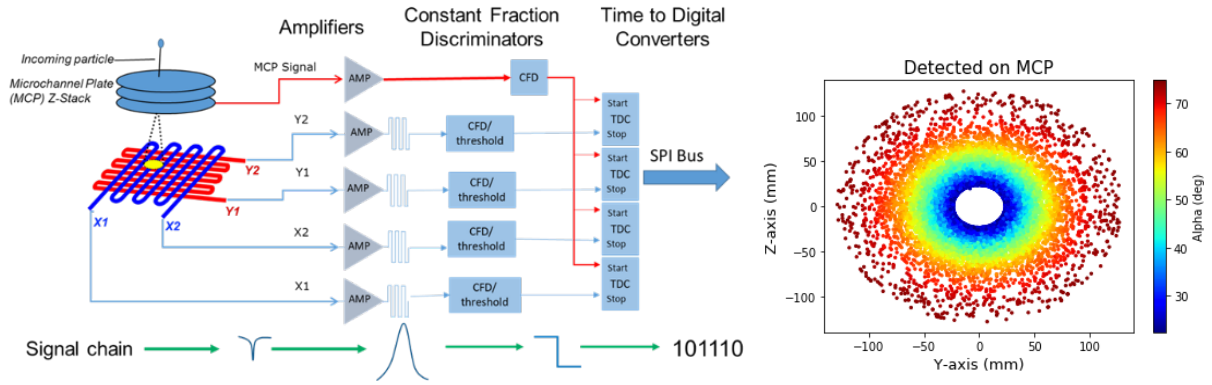

Fig. 7. XDL/MCP anode assembly and electronics functional schematic (left) and simulated ion detection points on the XDL anode (right).

The WPS design has been modified to fit within the mass and volume constraints of the ESRA 12U CubeSat platform and this reduced version of the design is colloquially referred to as the "WPS Wedge", as shown in Fig. 8. The WPS Wedge will measure ions with incident energies spanning 0.10–35 keV with targeted energy resolution $\Delta E/E \leq 0.15$. The instrument FOV is 89° × 60° with an angular resolution ≤ 10°.

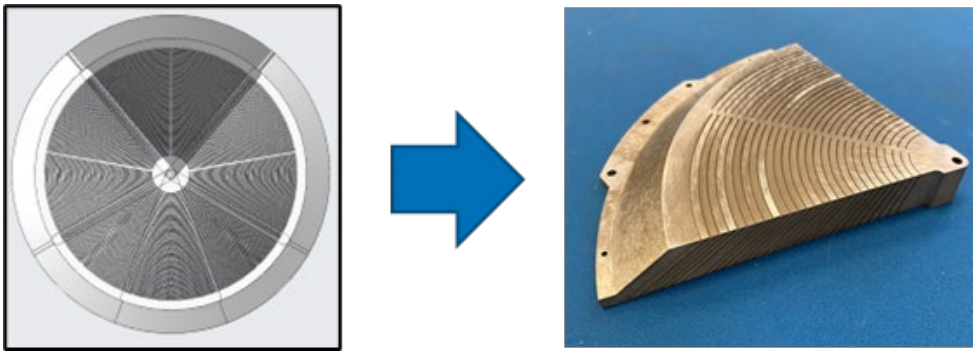

Fig. 8. For use on ESRA, the cylindrical WPS instrument (left) has been reduced to a wedge (right).

5. CRITICAL SUBSYSTEMS

As a DemVal mission, ESRA will also rapidly increase the TRL of next generation critical subsystems. These include a CubeSat compatible high voltage power supply, distributed processing architecture, payload processor, and flight software architecture which are described in more detail in the literature [31, 32]. The LANL-designed payload processor will control the experiment, record the data, and communicate with the CubeSat avionics while a DPM will provide limited processing at the sensor head locations and packetize data. The HVPS system will provide static and dynamic high voltage to the sensor payloads and the Flight Software (FSW) will control command & data handling. The top-level block diagram of the ESRA system is shown in Fig. 9.

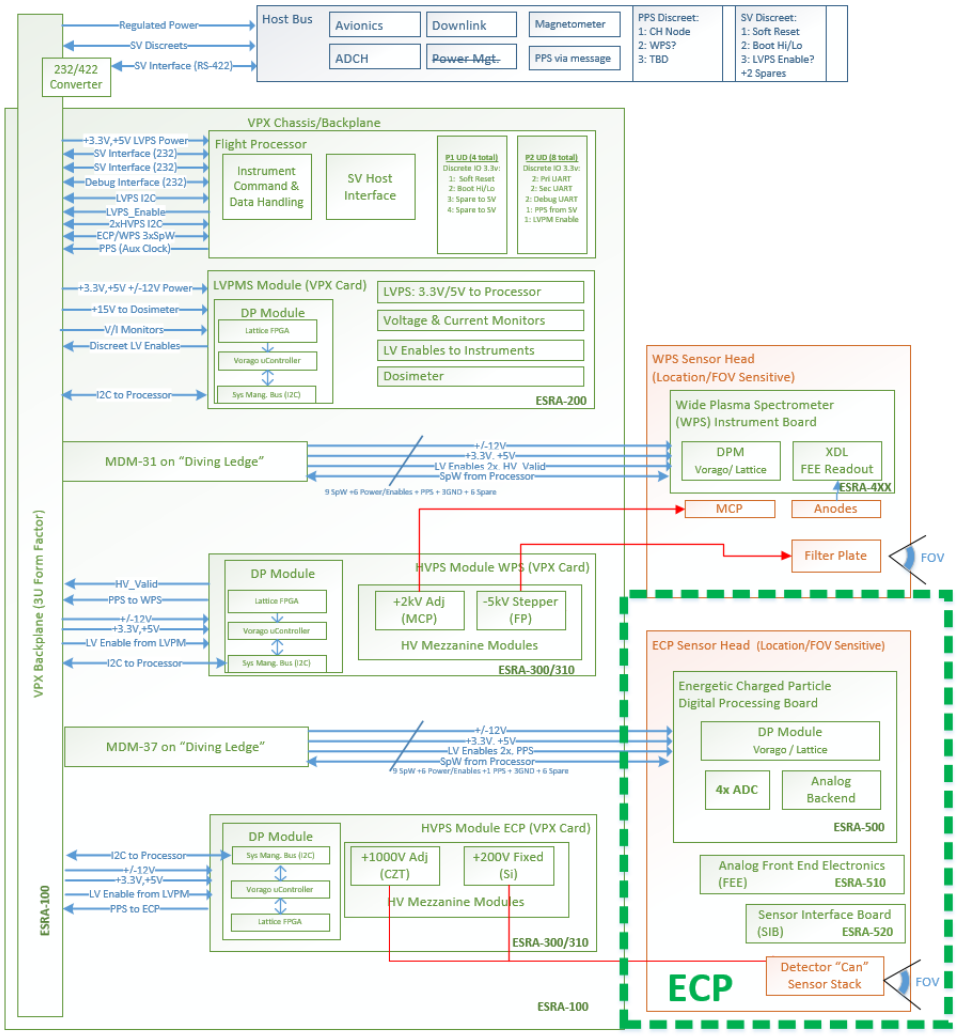

Fig. 9. ESRA Top Level System Block Diagram.

High Voltage Power Supply (HVPS)

The Space High Voltage Power Supply team at LANL is currently designing a new compact modular HVPS that will adhere to the 3U SpaceVPX (ANSI/VITA 78) specification using a conduction-cooled frame compliant with VITA 48. The HVPS will be integrated into ESRA 12U CubeSat to provide static and dynamic high voltage potentials to drive the ECP and WPS space environment sensors. The ECP sensor requires static high voltage to provide operational bias to the solid-state detectors. The WPS requires a stepping high voltage supply to sweep the EA filter plate and static voltages to bias the MCP and transmissive grid. The HVPS has been designed to meet radiation hardness requirements for operation in GTO by employing radiation hardened components with >100 kRad (Si) tolerance.

Distributed Processing Module (DPM)

The ESRA mission serves as a risk-reduction flight for the distributed architecture concept [31, 32]. Although ESRA is a 12U CubeSat with sensors and subsystems co-located, the WPS and ECP sensors are designed as "smart" sensors to prove out the distributed concept. The DPM is essentially a re-usable reference design for low-power digital electronics at the sensor head. The DPM provides the ability to mount multiple sensors in nontraditional configurations, i.e. sensor heads are not co-located, in order to maximize the ability to conform the sensor suite to any host and optimize fields-of-view. Space system architectures traditionally utilize a backplane in an enclosure to provide a central hub for command, data handling, processing, and power distribution. The traditional enclosure can be split into physically separated sub-instruments that stand-alone mechanically and are tethered to a smaller less resource-intensive hub. This is analogous to a modern office computer and its tethered USB peripherals. This distributed architecture concept provides flexibility and adaptability when integrating to mechanical and electrical

requirements of a particular host. A distributed system adds more modularity and the flexibility to add or subtract individual sub-instruments (such as space environment sensors) from an instrument payload without leaving empty backplane slots in a larger enclosure. Furthermore, this distributed processing concept enables "smart" sensors – self-contained sensors with data processing at the head, which are easier to test, integrate and re-use.

Payload Processor
The ESRA payload processor is a combination of 3U SpaceVPX and OpenVPX Architecture based on an existing LANL 6U design, enabling design reuse for firmware and flight software [48, 49, 50, 51]. The design employs a compact 3U Eurocard and Open/SpaceVPX architecture to reduce form factor while increasing performance. The reduction in size is critical for implementation on nano- and micro-satellite platforms such as the ESRA bus. The OpenVPX portion of the ESRA payload processor enables easier firmware and software development and testing by providing compatibility with cheaper commercial chassis, while the SpaceVPX portion allows for Space-Wire connectivity and critical signal redundancy. The heart of the payload processor is the GR740 LEON4 SPARC V8 processor from Cobham/Gaisler. It is capable of gigaflop performance at the nominal 250 MHz clock rate. One Gbyte of synchronous dynamic random-access memory (SDRAM) with 512 Mbytes of EDAC, clocked at 25 MHz, is addressed by the processor for volatile program and data storage. Eight Mbytes of nonvolatile Magnetoresistive Random-Access Memory (MRAM) are also included for nonvolatile program memory storage.

Flight Software (FSW)
The ESRA FSW running on the Gaisler LEON4 payload processor is based on a modular publish-subscribe architecture. The foundation of the FSW is a message bus created by LANL's internally-funded Cubesat Reusable Interface Software Platform (CRISP) project [52] which provides an extremely lightweight architecture that supports messaging to and from all the different components of the software system. The message passing architecture has been extended to seamlessly communicate with the DPM over SpaceWire to the WPS and ECP smart sensors, and via I2C to the HVPS sub-system. The ESRA FSW on the Gaisler LEON4 payload processor has been designed to be modular and reusable, allowing future LANL missions to focus on mission-specific software components while simply reusing the existing capabilities from ESRA/CRISP. The ESRA payload processor FSW provides the command and data handling functionality for the entire payload and has been designed to tolerate upsets and reboots of the space vehicle. Science data, state of health, and log data are stored in both volatile SDRAM and mirrored to a non-volatile flash drive. Various payload configuration parameters are held in non-volatile MRAM along with a ground configurable time-tagged sequence of commands. By managing the commands and data in the payload's radiation tolerant memories, ESRA is better prepared for unexpected upsets to the space vehicle.

The space vehicle (SV) interface of the ESRA payload processor FSW has met the specifications of the NanoAvionics 12U CubeSat spacecraft bus. The SV interface communicates with the NanoAvionics bus using the CubeSat Space Protocol (CSP). This lightweight network layer delivery protocol is used to transmit and receive messages with the CRISP message bus. These messages can be commands coming from the ground or payload telemetry being sent to the ground. The ESRA FSW leverages an open-source CSP library developed at Aalborg University and nanosatellite provider GomSpace. The ESRA FSW running on the Vorago VA41630 Arm Cortex-M4 in each instance of the DPM is built on top of the FreeRTOS real-time operating system. The DPM in the WPS and ECP sensors communicate with the payload processor over Space-Wire and the DPM in the HVPS and LVPM sub-systems communicate with the payload processor via I2C.

6. RADIATION ENVIRONMENT

The ESRA flight vehicle will transit the radiation belts twice per day with each passage through the outer radiation belt taking ~90 min and each passage of the inner radiation belt taking ~30 min. Note, these are approximations and the actual transit times will depend on the width of the belts which are dependent on geomagnetic activity. A plot of the ESRA orbit as a function of altitude, time, and location of the radiation belts is shown in Fig. 10(a). During these transits, the bus will be subjected to the energetic particle flux of the trapped radiation belts. As a result, the ESRA system will experience high levels of Total Ionizing Dose (TID).

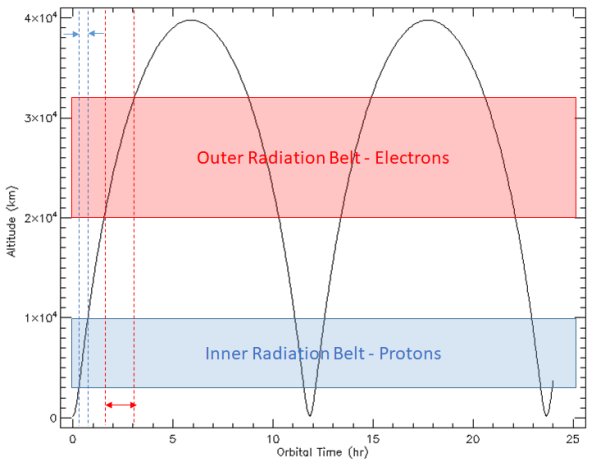

Fig. 10. Schematic of ESRA orbit as a function of orbital altitude, time, and approximate radiation belt locations.

To mitigate the effects of the natural radiation environment with regard to vehicle avionics, sensor payload, and critical subsystem performance there are two design options: 1) increase the part tolerance by implementing radhard parts to meet expected dose and 2) use shielding to lower the expected dose to meet part tolerance. The ESRA design principle utilizes a combination of both options since as a DemVal the subsystems designs use radhard and rad-tolerant parts with ratings greater than 100 krad. However, since the mission paradigm is to rapidly develop and deploy a pathfinder DemVal mission using commercial vendors the aluminum radiation shielding panels are being optimized to ensure the ESRA electronics are shielded such that they receive less than 20 krad/year. The shielding optimization effort implemented commercial FASTRAD radiation transport software package to assess the accumulated TID for a one year mission as a function of shielding thickness and location within the bus. The software package was used to propagate the energetic particle flux through the ESRA CAD model with 75 detectors distributed throughout the CAD model to measure TID. The three shielding cases analyzed are: 1) all 5 mm thick panels (ESRA124S2), 2) all 4 mm thick panels with 3 mm on ESRA card cage, shown as red panels in Fig. 11(right) (ESRA125S2), and 3) same as 2) but with 5 mm thick panel added to the -Z side. The initial shielding optimization result for case 3) indicates TID of less than 10 krad/year with a few locations receiving ~15 krad/year and a shielding mass is ~2 kg.

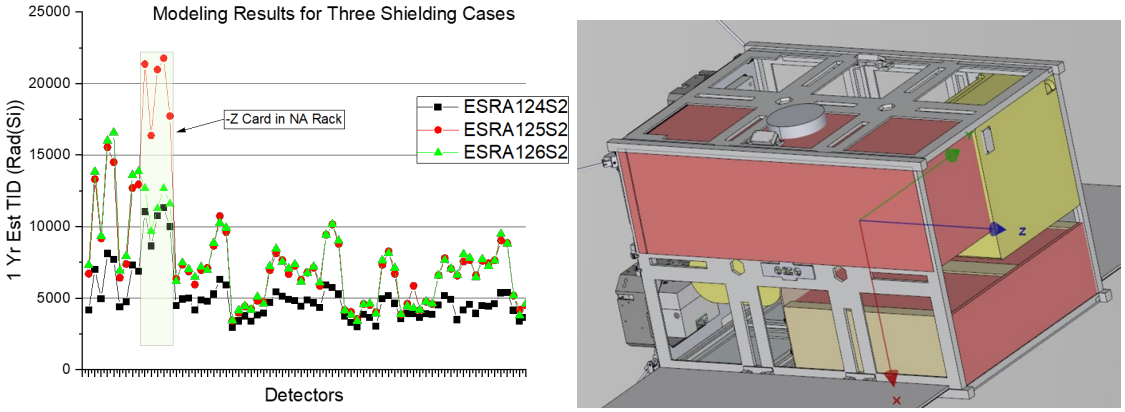

Fig. 11. FASTRAD calculation results for a 1-year mission using three shielding cases with TID at detector tally points scattered through the ESRA CAD model.

7. CONCLUSION

The ESRA mission is a part of a new era of science missions that are achieving "big science using small platforms." Similarly scoped CubeSat missions include CUSP [53], GTOSat [22], CeREs [20], CAPSTONE [54], CSSWE [21], MinXSS [55], MarCO [56], LunaH-Map [57], ASTERIA [58], and MAMBO [59] to name a few. Note, this is not an all-inclusive list given the extent and rapidly increasing number of CubeSat missions and is merely meant to highlight the range of scientific missions. Of particular interest, is the implementation of CubeSat missions beyond LEO, e.g.

MarCO as the first interplanetary mission, CAPSTONE as the first cislunar mission, GTOSat as the first through the radiation belts, and ESRA which will follow GTOSat. The ESRA mission will fly through GTO while making observations of the charged particle populations in the Earth's radiation belts. This will allow for the demonstration and validation of the next generation space environment sensors and critical subsystems. A commercial satellite bus supplied by NanoAvionics will host the WPS and ECP sensors along with the critical subsystems such as the HVPS, DPM, and Payload Processor. The mission launch and integration are being provided by the DoD Space Test Program with an anticipated GTO insertion in late 2024. The desired orbital parameters include perigee of 200 km, apogee of 36,000 km, and inclination of 40° ±20°. The commercial space sector continues to increase the capability of SmallSat platforms and ground stations while simultaneously reducing risk and cost. The ESRA mission leverages this capability by partnering with NanoAvionics, thus allowing the mission team to focus primarily on payload development.

8. ACKNOWLEDGEMENTS

The research conducted at Los Alamos National Laboratory was under the auspices of the Department of Energy.

9. REFERENCES

[1] D. Young, "Space plasma particle instrumentation and the new paradigm: Faster, cheaper, better," in *Measurement Techniques in Space Plasmas: Particles*, R. Pfaff, J. Borovsky and D. Young, Eds., Geophysical Monograp Series 102, 1998, pp. 1-16.

[2] H. Spence, K. Klein and J. Bookbinder, "The HelioSwarm Mission: A Swarm of Small Satellites Revealing the Physics of Space Plasma Turbulence," in *Proceedings of the 33rd Annual Small Satellite Conference*, Logan, UT, 2019.

[3] E. Friis-Christensen, H. Luhr, D. Knudsen and R. Haagmans, "Swarm—An Earth Observation Mission Investigating Geospace," *Advances in Space Research,* vol. 41, no. 1, p. 210–216, 2008.

[4] E. MacDonald, H. Funsten, E. Dors, M. Thomsen, P. Janzen, R. Skoug, G. Reeves, J. Stenberg, R. Harper, D. Young, J.-M. Jahn and D. Reisenfeld, "New Magnetospheric Ion Composition Measurement Techniques," 2009.

[5] P. Fernandes, H. Funsten, E. Dors, R. B. Harper, E. MacDonald, D. Reisenfeld, R. Skoug, J. Steinberg and M. Thomsen, "Low-Resource Technique for Measurement of H+ and O+ in the Terrestrial Magnetosphere," *J. Geophys. Res.:Space Physics,* vol. 124, p. 9137–9153, 2019.

[6] H. Funsten and D. McComas, "Limited resource plasma analyzers:Miniaturization concepts," in *Measurement Techniques in Space Plasmas: Particles*, R. Pfaff, J. Borovsky and D. Young, Eds., AGU Monograph Series, 1998, pp. 157-167.

[7] C. Maldonado, M. McHarg, R. Balthazor and R. Osiander, "Undergraduate research and science mission opportunities with microtechnology enabled particle detectors," in *Proc. SPIE 10982, Micro- and Nanotechnology Sensors, Systems, and Applications XI, 109820I*, Baltimore, 2019.

[8] K. Ogasawara, D. George, J. Goldstein, K.-J. Hwang, Y. Nishimura, D. A. Ruggles and J. Stange, "3DI: A novel ion composition and three-dimensional velocity analyzer for the topside ionosphere," *Scientific Reports,* vol. 10, no. 1, pp. 1-13, 2020.

[9] R. Fausch, P. Wurz, M. Tulej and U. Rohner, "CubeSatTOF: Planetary Atmospheres Analyzed with a 1U High-Performance Time-Of-Flight Mass Spectrometer," in *Proceedings of teh 34th Annual Small Satellite Conference*, Logan, UT, 2020.

[10] C. Maldonado, G. Wilson, J. McGlown, H. Morning, D. Arnold, D. Reisenfeld and M. Holloway, "An Ultra-Low Resource Ion Mass Spectrometer for CubeSat Platforms," in *Proceedings of the 36th Annual Small Satellite Conference*, Logan, UT, 2021.

[11] L. Fanelli, S. Noel, G. D. Earle, C. Fish, R. L. Davidson, R. V. Robertson, P. Marquis, V. Garg, N. Somasundaram, L. Kordella and P. Kennedy, "A versatile retarding potential analyzer for nano-satellite platforms," *Rev. Sci. Instrum.,* vol. 86, p. 124501, 2015.

[12] C. A. Maldonado, Z. Eyler, B. Pierce, L. Matson, P. Neal, H. Richards, R. L. Balthazor, J. Harley and M. G. McHarg, "A laminated energetic electrostatic analyzer for 0-5 keV charged particles," *Rev. Sci. Instrum.,* vol. 91, no. 1, 2020.

[13] H. Feldmesser, M. Darrin, R. Osiander, L. Paxton, A. Rogers, J. Marks, M. McHarg, R. Balthazor, L. Krause and J. Fitzgerald, "Canary: ion spectroscopy for ionospheric sensing," in *Proc. SPIE, Space Missions and Technologies*, Orlando, FL, United States, 2010.

[14] D. M. Wesolek, J. L. Champion, F. A. Herrero, R. Osiander and R. L. Champion, "A micromachined flat plasma spectrometer," in *Proc. SPIE 5344, MEMS/MOEMS Components and their Applications*, 2004.

[15] C. A. Maldonado, D. Reisenfeld, P. Fernandes, B. Larsen, G. Wilson, R. L. Balthazor, C. Enloe and M. G. McHarg, "The effects of spacecraft potential on ionospheric ion measurements," *Journal of Spacecraft and Rockets,* vol. 58, no. 6, pp. 1704-1713, 2021.

[16] C. Maldonado, R. Cress, P. Gresham, J. Armstrong, G. Wilson, D. Reisenfeld, B. Larsen, R. Balthazor, J. Harley and M. McHarg, "Space radiation dosimetry using the integrated Miniaturized Electrostatic Analyzer - Reflight (iMESA-R)," *Space Weather,* 2020.

[17] L. Kepko, C. Clagett, L. Santos, B. Azimi, D. Berry, T. D. Bonalsky, M. Colvin, A. Cudmore, A. Evans, S. Hesh, S. Jones, J. Marshall, N. Paschalidis, Z. Peterson, M. Rodriquez, S. Sheikh, S. Starin and E. Zesta, "Dellingr: NASA Goddard Space Flight Center's first 6U spacecraft," in *Proceedings of the 31st AIAA/USU Small Satellite Conference*, Logan, UT, 2017.

[18] J. E. Nordholt, D. B. Reisenfeld, R. C. Wiens, S. P. Gary, F. Crary, D. M. Delapp, R. C. Elphic, H. O. Funsten, J. J. Hanley, D. J. Lawrence, D. J. McComas, M. Shappirio, J. T. Steinberg, J. Wang and D. T. Young, "Deep Space 1 encounter with Comet 19P/Borrelly: Ion compositionmeasurements by the PEPE mass spectrometer," *Geophysical Research Letters,* vol. 30, no. 9, pp. 1465-, 2003.

[19] E. MacDonald, K. Lynch, M. Widholm, R. Arnoldy, P. Kintner, E. Klatt, M. Samara, J. LaBelle and G. Lapenta, "In situ measurements of thermal electrons on the SIERRA nightside auroral sounding rocket," *J. of Geophys. Res.,* vol. 111, no. A12310, 2006.

[20] S. G. Kanekal, L. Blum, E. R. Christian, G. Crum, M. Desai, J. Dumonthier, A. Evans, A. Greeley, S. Guerros, S. Livi, K. LLera, J. Lucas, J. MacKinnon, J. Mukherjee, K. Ogasawara, N. Paschalidis, D. Patel, E. Pollack, S. Riall, Q. Schiller, G. Suarez and E. J. Summerlin, "The MERiT Onboard the CeREs: A Novel Instrument to Study Energetic Particles in the Earth's Radiation Belts," *Journal of Geophysical Research: Space Physics,* vol. 124, p. 5734–5760, 2019.

[21] X. Li, Q. Schiller, L. Blum, S. Califf, H. Zhao, W. Tu, D. Turner, D. Gerhardt, S. Palo, S. Kanekal, D. Baker, J. Fennell, J. Blake, M. Looper, G. Reeves and H. Spence, "First results from CSSWE CubeSat: Characteristics of relativistic electrons in the near-Earth environment during the October 2012 magnetic storms," *Journal of Geophysical Space Research: Space Physics,* vol. 118, p. 6489–6499, 2013.

[22] L. W. Blum, L. Kepko, D. Turner, C. Gabrielse, A. Jaynes, S. Kanekal, Q. Schiller, J. Espley, D. Sheppard, L. Santos, J. Lucas and S. West, "The GTOSat CubeSat: scientific objectives and instrumentation," in *Proceedings Volume 11389, Micro- and Nanotechnology Sensors, Systems, and Applications XII*, Baltimore, MA, 2020.

[23] R. Cress, C. Maldonado, M. Coulter, K. Haak, R. Balthazor, M. McHarg, D. Barton, K. Greene and C. Lindstrom, "Calibration of the Falcon Solid-state Energetic Electron Detector (SEED)," *Space Weather,* vol. 18, no. 5, pp. 1-7, 2020.

[24] C. Escoubet, R. Schmidt and M. Goldstein, "Cluster - Science and Mission Overview," in *The Cluster and Phoenix Missions*, Dordrecht, Springer, 1997, pp. 11-32.

[25] J. L. Burch, T. E. Moore, R. B. Torbert and B. L. Giles, "Magnetospheric Multiscale Overview and Science Objectives," *Space Science Reviews,* vol. 199, pp. 5-21, 2016.

[26] V. Angelopoulos, "The THEMIS mission," *Space Science Review,* vol. 141, pp. 5-34, 2008.

[27] J. C. McDowell, "The Low Earth Orbit Satellite Population and Impacts of the SpaceX Starlink Constellation," *The Astrohpysical Journal Letters,* vol. 892, no. 2, pp. 1-10, 2020.

[28] J. Radtke, C. Kebschull and E. Stoll, "Interactions of the space debris environment with mega constellations—Using the example of the OneWeb constellation," *Acta Astronautica,* vol. 131, pp. 55-68, 2017.

[29] D. Tournear, "Future Directions: Delivering Capabilities," in *Proceedings of the Small Satellite Conference, SSC20-IV-02*, Logan, UT, 2020.

[30] A. Klesh, B. Clement, C. Colley, J. Essmiller, D. Forgette, J. Krajewski, A. Marinan, T. Martin-Mur, J. Steinkraus, D. Sternberg, T. Werne and B. Young, "MarCO: Early Operations of the First CubeSats to Mars," in *32nd Annual AIAA/USU Conference on Small Satellites*, Logan, UT, 2018.

[31] C. A. Maldonado, J. Deming, B. N. Mosley, K. S. Morgan, J. McGlown, A. Nelson, P. Fernandes, M. Kroupa, K. Katko, M. P. HHehlen, D. Arnold, J. Barney, C. Safi, M. Pyle, T. Schultz, D. Reisenfeld, R. Skoug, A. Guider, M. Holloway, H. Morning, E. Krause, B. Sandoval, D. Beckman, Z. Miller, R. Merl, P. S. Graham, T. P. White, Z. Tripp, B. Hoose, C. Roecker, A. Klimenko, R. Dutch, K. Kaufeld, E. Cox, Q. Cole, C. Clanton, P. Bloser, B. A. Larsen, T. Fairbanks, J. George and J. Michel, "The Experiment for Space Radiation Analysis: A 12U CubeSat to Explore the Earth's Radiation Belts," in *IEEE Aerospace Conference*, Big Sky, MT, 2022.

[32] C. Maldonado et al., "The Experiment for Space Radiation Analysis: Probing the Earth's Radiation Belts Using a CubeSat Platform," in *Proceedings of the 36th Annual Small Satellite Conference*, Logan, UT, 2021.

[33] C. Alsop, S. Scott and L. Free, "UV Rejection Design and Performance of the PEACE Electrostatic Analyzers," in *Measurement Techniques in Space Plasma: Particles*, J. B. D. Y. R.F. Pfaff, Ed., Geophysical Monograph Series, American Geophysical Union, 1998, p. 269–274.

[34] V. Venkataraman, R. Satheesh Thampi, J. K. Abhishek, A. N. Aneesh, A. M. Pillai, A. Dey and A. Rajendra, "Development of Space Qualified High Solar Absorptance Nanostructured Black CuO Coating for Spaceborne Plasma Instruments," *Journal of Materials Engineering and Performance,* vol. 31, no. 7, pp. 5689-5696, 2022.

[35] T. H. Zurburchen, P. Bochsler and F. Scholze, "Reflection of ultraviolet light at 121.6 nm from rough surfaces," *Optical Engineering,* vol. 34, no. 5, 1995.

[36] D. J. Gershman and T. H. Zurburchen, "Modeling extreme ultraviolet suppression of electrostatic analyzers," *Rev. Sci. Instrum.,* vol. 81, p. 045111, 2010.

[37] E. S. Elshazly, G. Tepper and A. Burger, "Charge trapping in detector grade thallium bromide and cadmium zinc telluride: Measurement and theory," *Nuclear Instruments and Methods in Physics Research Section A: Accelerators, Spectrometers, Detectors and Associated Equipment,* vol. 620, no. 2-3, pp. 279-284, 2010.

[38] J. Barney, D. Arnold, O. Garduno, M. Kroupa, C. A. Maldonado, Z. Miller, C. Roecker, D. Wakeford and B. A. Larsen, "Experiment for Space Radiation Analysis, Energetic Charged Particle Sensor: a Charged Particle Telescope with Novel Sensors for Measuring the Earth's Radiation Belts," in *Proceedings of the IEEE Aerospace Conference*, Big Sky, MT, 2022.

[39] S. Agostinelli et al., "Geant4—a simulation toolkit," *Nuclear Instruments and Methods in Physics Research Section A: Accelerators, Spectrometers, Detectors and Associated Equipment,* vol. 506, no. 3, pp. 250-303, 2003.

[40] R. M. Skoug, H. O. Funsten, E. Möbius, R. H. Harper, K. H. Kihara and J. S. Bower, "Awidefield of view plasma spectrometer," *J. Geophys. Res. Space Physics,* vol. 121, p. 6590–6601, 2016.

[41] D. Dahl, "SIMION for the personal computer in reflection," *Int. J. Mass Spectrom.,* vol. 200, no. 3, 2000.

[42] R. M. Skoug, H. O. Funsten, E. Mobius, R. W. Harper, K. H. Kihara and J. S. Bower, "A wide field of view plasma spectrometer," *J. Geophys. Res. Space Physics,* vol. 121, pp. 6590-6601, 2016.

[43] O. Siegmund, M. Gummin, J. Stock, G. Naletto, G. Gaines, R. Raffanti, J. S. Hull, R. Abiad, T. Rodriguez-Bell, T. Magoncelli, P. Jelinsky, W. Donakowski and K. Kromer, "Performance of the double delay line microchannel plate detectors for the Far-Ultraviolet Spectroscopic Explorer," in *Proc. SPIE 3114, EUV, X-Ray, and Gamma-Ray Instrumentation for Astronomy VIII*, San Diego, CA, 1997.

[44] O. Siegmund, P. Jelinsky, J. Stock, J. Hull, D. Doliber, J. Zaninovich, A. Tremsin and K. Kromer, "High resolution cross delay line detectors for the GALEX mission," in *Proc. SPIE 3765, EUV, X-Ray, and Gamma-Ray Instrumentation for Astronomy X*, Denver, CO, United States, 1999.

[45] J. Stock, O. Siegmund, J. Hull, K. Kromer, S. Jelinsky, H. Heetderks, M. Lampton and S. Mende, "Cross-delay-line microchannel plate detectors for the Spectrographic Imager on the IMAGE satellite," in *Proc. SPIE 3445, EUV, X-Ray, and Gamma-Ray Instrumentation for Astronomy IX*, San Diego, CA, United States, 1998.

[46] O. Siegmund, M. Gummin, T. Sasseen, P. Jelinsky, G. Gaines, J. Hull, J. Stock, M. Edgar, B. Welsh, S. Jelinsky and J. Vallerga, "Microchannel plates for the UVCS and SUMER instruments on the SOHO

satellite," in *Proc. SPIE 2518, EUV, X-Ray, and Gamma-Ray Instrumentation for Astronomy VI*, San Diego, CA, United States, 1995.

[47] J. Vallerga, J. Zaninovich, B. Welsh, O. Siegmund, J. McPhate, J. Hull, G. Gaines and D. Buzasi, "The FUV detector for the cosmic origins spectrograph on the Hubble Space Telescope," *Nuclear Instruments and Methods in Physics Research, Section A,* vol. 477, no. 1-3, pp. 551-555, 2002.

[48] R. Merl and P. Graham, "Radiation-Hardened SpaceVPX System Controller," in *2018 IEEE Aerospace Conference*, Big Sky, MT, 2018.

[49] R. Merl and P. Graham, "MicroTCA for Space Applications," in *2016 IEEE Aerospace Conference*, Big Sky, MT, 2016.

[50] R. Merl, E. Cox, R. Dutch, P. Graham, S. Larsen, J. Michel, J. Milby, K. Morgan and K. Tripp, "LEON4 Based Radiation-Hardened SpaceVPX System Controller," in *2020 IEEE Aerospace Conference*, Big Sky, MT, 2020.

[51] R. Merl and P. Graham, "A low-cost, radiation-hardened single-board computer for command and data handling," in *2016 IEEE Aerospace Conference*, Big Sky, MT, 2016.

[52] R. Scobie, K. Kaufeld, B. Hoose, K. Morgan, K. Katko, M. Hehlen and J. Michel, "CubeSat Reusable Interface Software Platform (CRISP): A Lightweight Message-Bus-Based Flight Software Architecture for Rapid Payload Integration," in *Proceedings of the 36th Annual Small Satellite Conference*, Logan, UT, 2021.

[53] M. Desai, F. Allegrini, R. Ebert, K. Ogasawara, M. Epperly, D. George, E. Christian, S. Kanekal, N. Murphy and B. Randol, "The CubeSat Mission to Study Solar Particles," *IEEE Aerospace and Electronic Systems Magazine,* vol. 34, no. 4, pp. 16-28, 2019.

[54] T. Gardner, B. Cheetham, A. Forsman, C. Meek, E. Kayser, J. Parker, M. Thompson, T. Latchu, R. Rogers, B. Bryant and T. Svitek, "CAPSTONE: A CubeSat Pathfinder for the Lunar Gateway Ecosystem," in *Proceedings of the 35th Annual AIAA/USU Small Satellite Conference*, Logan, UT, 2021.

[55] J. Mason, T. Woods, A. Caspi, P. Chamberlin, C. Moore, A. Jones, R. Kohnert, X. Li, S. Palo and S. Solomon, "Miniature X-Ray Solar Spectrometer: A Science-Oriented, University 3U CubeSat," *Journal of Spacecraft and Rockets,* vol. 53, no. 2, pp. 328-339, 2016.

[56] A. Klesh, B. Clement, C. Colley, J. Essmiller, D. Forgette, J. Krajewski, A. Marinan, T. Martin-Mur, J. Steinkraus, J. Sternberg, T. Werne and B. Young, "MarCO: Early Operations of the First CubeSats to Mars," in *Proceedings of the 32nd Annual AIAA/USU Conference on Small Satellites*, Logan, UT, 2018.

[57] C. Hardgrove, J. DuBois, L. Heffern, E. Cisneros, J. Bell, T. Crain, R. Starr, T. Prettyman, I. Lazbin, B. Roebuck, N. Struebel, E. Clark, D. Nelson, J. Bauman, B. Williams, E. Johnson, J. Christian, G. Stoddard, M. Tsay, J. Model, P. Hruby, A. Babuscia, S. Stem, D. Sanders, E. Hegel, M. Wiens, S. Parlapiano, P. Hailey, T. O'Brien, K. Mesick and D. Coupland, "The Lunar Polar Hydrogen Mapper (LunaH-Map) Mission," in *Proceedings of the 33rd Annual AIAA/USU Conference on Small Satellites*, Logan, UT, 2019.

[58] M. Knapp, S. Seager, B. Demory, A. Krishnamurthy, M. Smith, C. Pong, V. Bailey, A. Donner, P. Pasquale, B. Campuzano, C. Smith, J. Luu, A. Babuscia, R. Bocchino, J. Loveland, C. Colley, T. Gedenk, T. Kulkarni, K. Hughes, M. White, J. Krajewski and L. Fesq, "Demonstrating High-precision Photometry with a CubeSat: ASTERIA Observations of 55 Cancri e," *The Astronomical Journal,* vol. 160, no. 23, 2020.

[59] P. Bloser, W. Vestrand, M. Hehlen, L. Parker and A. Hoover, "The Mini Astrophysical MeV Background Observatory (MAMBO) CubeSat mission," in *Proc. SPIE 11444, Space Telescopes and Instrumentation 2020: Ultraviolet to Gamma Ray*, Online Only, 2020.